INFORMATICS IN BIOLOGY, HEALTH, AND FOOD

Interdisciplinary Explorations in Life Science

Volume 1. Number 1, Dec. 2024 DOI: 10.22034/ibhf.2024.208761

Original Article

Molecular Dynamic Simulation of HIV-1 Protease, Integrase and Reverse Transcriptase with Delta-9-tetrahydrocannabinol and Curcumin as two Herbal Ligands

Samaneh Esmaeili Shikhabad[1]*, Hamid Mosaddeghi[1], Fatemeh Ravari [1]

[1] Department of Chemistry, Payame Noor University, Tehran 19395-4697, Iran.

Received: 2024/09/27, **Accepted:** 2024/10/28; **Online Published:** 2024/10/31

Abstract

The HIV-1 virus has three important enzymes: protease, reverse transcriptase, and integrase, which are essential for vital functions. The Acquired immunodeficiency syndrome (AIDS) virus causes a significant number of deaths annually. Herbal drugs, are inexpensive, with minimal side effects, and have been used for many years alongside conventional medicine. In fact, herbal medicine forms the basis of modern pharmacology. In this study, we investigated the potential of two herbal compounds, Curcumin (CRC) and Delta-9-Tetrahydrocannabinol (THC), as inhibitors of HIV-1. After conducting 100 nanoseconds (ns) of molecular dynamics (MD) simulations for systems involving each of these three proteins in the presence of the ligands, we analyzed the simulated systems. The results, including root-mean-square deviations (RMSD), radius of gyration (Rg), root-mean-square fluctuation (RMSF), solvent accessible surface area (SASA), dictionary of secondary structure of proteins (DSSP), and g_mmpbsa, indicate that both ligands can bind to the active sites of the proteins and inhibit HIV-1 activity. These MD simulation results suggest that both CRC and THC are effective inhibitors of HIV-1.

Keywords: Curcumin, Molecular Dynamics Simulation (MD Simulation), HIV-1, Protease, Integrase, Reverse Transcriptase.

Cite this article: Molecular Dynamic Simulation of HIV-1 Protease, Integrase and Reverse Transcriptase with Delta-9-tetrahydrocannabinol and Curcumin as two Herbal Ligands. *Informatics in Biology, Health, and Food*. 2024 Dec;1(1):91-104.

Corresponding author: Samaneh Esmaeili Shikhabad **Email**: esmasamaneh@gmail.com

Introduction

Human Immunodeficiency Virus type 1 (HIV-1) is a retrovirus that infects the cells of the human immune system and is responsible for the onset of the disease known as acquired immunodeficiency syndrome (AIDS) (1). HIV-1 has three enzymes essential for its replication cycle: protease (PR), integrase (IN), and reverse transcriptase (RT). Consequently, these three proteins are the primary targets for most anti-HIV drug development efforts (2). IN catalyzes the integration of viral DNA into the human genome, which increases viral stability and ensures persistent infection (3-6). Structurally, HIV-1 integrase consists of three distinct domains: the N-terminal domain (residues 1–50): contains four α-helices, the central domain protease-resistant (residues 50–212), and the C-terminal region (residues 212–288), which forms a five-stranded β-sheet (3). The structure of HIV-1 integrase has been resolved by X-ray crystallography (7).

HIV-1 reverse transcriptase (RT) is a crucial target for anti-AIDS drugs. RT converts single-stranded viral RNA into double-stranded (ds) DNA, which is subsequently integrated into the host genome. The enzymatic activities of RT include: (1) RNase H (RNH), and (2) DNA polymerase, which can use either DNA or RNA as a template. RT is composed of two subunits: p66 (66 kDa) and p51 (51 kDa), both of which contain four polymerase subdomains: thumb, palm, fingers, and connection (8). The crystal structure of HIV-1 protease (PR) has been determined. The two chemically identical subunits of the PR dimer are arranged nearly symmetrically. Each subunit folds into a compact structure of β-strands with a short α-helix near the C terminus. Residues 44–57 form a flap composed of antiparallel β-strands (9). The active site of the protease is located at the dimer interface (10). HIV-1 protease, a member of the aspartyl protease family, is composed of two identical subunits, each containing 99 amino acids. (11). The interaction between protein-protein or protein-ligand molecules is a critical step in many biological processes. In the case of the HIV-1 protease, plays a fundamental role in producing the active components of the viral polyprotein, which must bind to the active site (12).

Molecular dynamics (MD) simulations are a powerful computational tool for studying the time evolution and dynamics of physicochemical systems at the molecular level, allowing for the determination of physical and chemical properties (13). The interactions of HIV-1 protease with ligands have been extensively studied by various computational methods, including molecular simulations and free energy calculation techniques, which are commonly employed for short timescales (14). For example, the molecular mechanics Poisson-Boltzmann surface area (MM-PBSA) method has been used to calculate binding affinities (15-17). In 2015, MD simulations of protein-ligand interactions were carried out by Hongtao Zhao and Amedeo Caflisch. Additionally, MD simulations have been performed after docking to predict the binding modes of top-ranking compounds as a final step in computational workflows, or to guide chemical synthesis for optimization (18). One important factor in predicting ligand binding is the thermodynamic properties of protein-ligand

interactions (19, 20). For years, scientists have debated various models to explain protein-ligand binding, including the lock and key, conformational selection, and induced-fit models. Understanding the underlying mechanisms of binding kinetics enhances our ability to design effective ligands.

In this study, we present the results of molecular dynamics simulations based on docking data from our previous work (21). These simulations involved three HIV-1 proteins and two herbal ligands: Dronabinol (a psychoactive compound extracted from the resin of Cannabis sativa [marijuana, hashish], with the isomer delta-9-tetrahydrocannabinol [THC] being the most active form, known for producing characteristic mood and perceptual changes), and Curcumin (a yellow-orange dye derived from turmeric, the powdered root of Curcuma longa [CRC]).

It is used in the preparation of curcuma paper and the detection of boron. Curcumin appears to possess a spectrum of pharmacological properties, due primarily to its inhibitory effects on metabolic enzymes. Molecular dynamics simulations were performed for 100 ns, and various analyses, including RMSD, RMSF, Rg, PCA, and GMMPBSA, were conducted. The results of each system were then compared to one another.

Materials and Methods

Molecular dynamics simulation

The MD simulations were performed using the GROMACS 5.1.4 software package with the AMBER 99sb force field (22, 23). The molecular topology files for the ligands were generated using the Antechamber program, and RESP charges were obtained from Gaussian (24,25). The simulation cell was a cubic periodic box. The box sizes for each system were as follows: for IN-CRC, 74 Å × 74 Å × 74 Å; for IN-THC, 73.4 Å × 73.4 Å × 73.4 Å; for PR-CRC and PR-THC, 81.3 Å × 81.3 Å × 81.3 Å; and for RT-CRC and RT-THC, 140 Å × 140 Å × 140 Å. The minimum distance between the box walls and the protein was set to be greater than 10 Å. To neutralize the total charge, two chloride ions were added for IN-CRC and IN-THC, four chloride ions for PR-CRC and PR-THC, and nine chloride ions for RT-CRC and RT-THC.

The total number of atoms in each system, including protein complexes and water molecules, was as follows: IN-CRC (39,906 atoms), IN-THC (39,123 atoms), PR-CRC (53,108 atoms), PR-THC (53,096 atoms), RT-CRC (271,382 atoms), and RT-THC (271,214 atoms). The TIP3P water model was used in the simulations (26).

The system was equilibrated through a 100 ns MD simulation at 310 K, with a time step of 2 fs. The primary calculation methods and parameters used during the MD simulation were as follows: the NPT (normal pressure and temperature) ensemble was applied with periodic boundary conditions (PBC) at 310 K. To maintain the temperature, the Berendsen thermostat was used. The isothermal compressibility was set to 4.5×10^{-5} bar^{-1}. Furthermore, the pressure was maintained at 1 bar using the Parrinello-Rahman scheme (27). Electrostatic interactions were calculated using the Particle Mesh Ewald (PME) method (28). The cut-off radius for van der Waals and Coulomb interactions was set to 1 nm, and periodic boundary conditions (PBC) were applied. The PME method was used to calculate long-range electrostatics (29).

Analysis of Trajectory

Molecular Mechanics Poisson−Boltzmann Surface Area (MM-PBSA) is a method used to calculate the free energies of interaction, implemented in GROMACS via the g_mmpbsa tool. Additionally, other GROMACS tools were used to analyze various parameters, such as the radius of gyration (g_gyrate), root-mean-square fluctuation (RMSF) (g_rmsf), root-mean-square deviation (RMSD) (g_rms), solvent accessible surface area (SASA) (g_sasa), and the Dictionary of Secondary Structure of Proteins (DSSP) (30,31). Principal Component Analysis (PCA) was performed to analyze the system's rotational and translational movements, which were removed using the g_covar tool from GROMACS to generate a covariance matrix. The eigenvalues and eigenvectors of this matrix were then calculated by diagonalizing it. The eigenvectors corresponding to the largest eigenvalues are referred to as "principal components," as they represent the largest amplitude collective movements. The main trajectory was filtered, and the most significant eigenvectors, namely vector 1 and 2, were analyzed using the g_anaeig and g_covar tools from GROMACS (32). Figures and images were generated using XMGRACE (Linux software), VMD, and Chimera (33-38).

2.3 Principal Component Analysis (PCA)

Principal Component Analysis (PCA) is a statistical technique that uses an orthogonal transformation to convert a set of possibly correlated variables into a set of linearly uncorrelated variables called principal components. The first principal component captures the largest variance in the data. In this method, the first principal component (PCA1) has the largest possible variance, and the PCA graph, which plots eigenvectors (PCA1 vs. PCA2 or eigenvectors 1 and 2), illustrates the maximum motion of the proteins.

Results

Molecular Dynamics Simulations

Root-mean-square deviations (RMSD)

Root-mean-square deviations (RMSD) for the HIV-1 protein systems bound to two herbal drugs were calculated to assess the convergence of the protein structure towards an equilibrium state after binding, during the 100 ns MD simulation. The RMSD plot was based on the Cα backbone atoms. The RMSD values for PR, PR-CRC, PR-THC, RT, RT-CRC, RT-THC, IN, IN-CRC, and IN-THC are shown in Figure 1.

As shown in Figure 1A, the RMSD of PR-THC stabilizes at approximately 0.22 nm after 80 ns. The RMSD of PR-CRC shows a peak at 35 ns, as at this point, CRC has not fully bound to the active site, resulting in greater instability. However, after this peak, the RMSD stabilizes around 0.17 nm, indicating that the structure reaches a relative equilibrium. Similar observations are made in Fig. 1B and 1C: the RMSD of RT-THC and RT-CRC stabilizes at approximately 0.3 nm, and the RMSD of IN-THC and IN-CRC stabilizes at about 0.2 nm. This suggests that, in both cases, the structures of the two systems reach a state of relative equilibrium.

As shown in Fig. 1, the binding of the two ligands (CRC and THC) to PR, RT, and IN leads to a decrease in RMSD and an increase in the stability of the complexes. Therefore, it can be concluded that the ligands bind to the active sites, potentially inhibiting the activity

of HIV-1. Similar studies have also shown that protein binding to ligands reduces the RMSD (39.40).

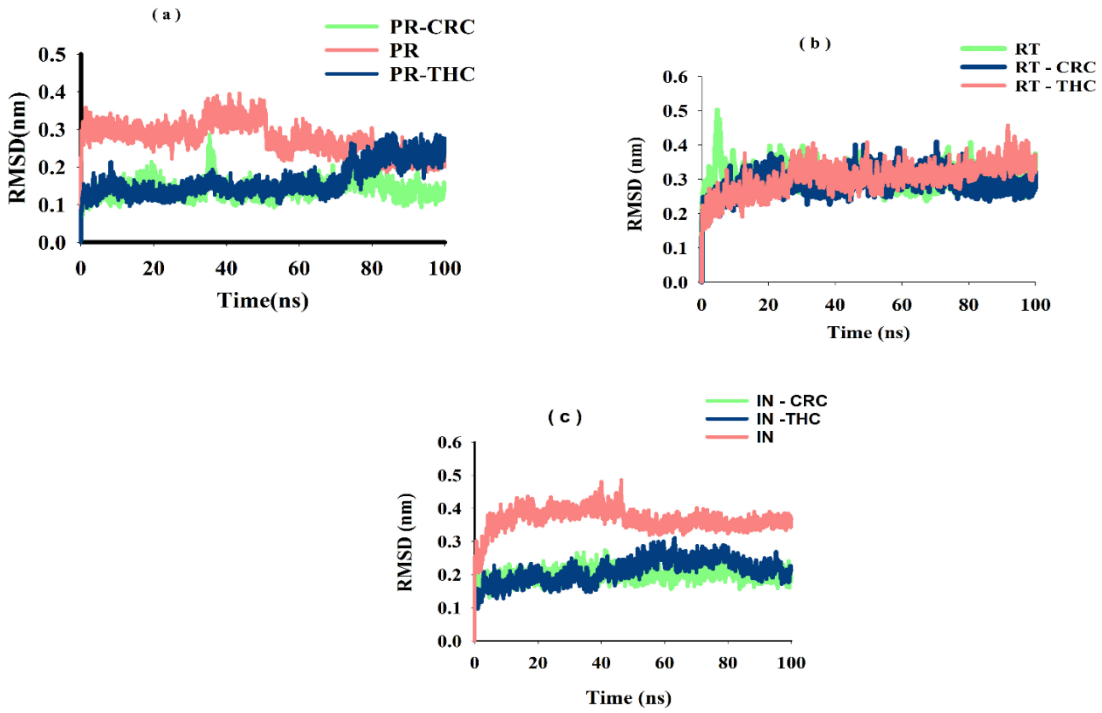

Figure 1: RMSD (a) PR, PR-CRC and PR-THC (b) RT, RT-CRC and RT-THC (c) IN, IN-CRC and IN-THC.

Radius of gyration (Rg)

The radius of gyration (Rg) is defined as the radial distance of a point from the axis of rotation at which its moment of inertia about that axis would be the same as with its actual distribution of mass. Rg is an important parameter that indicates the compactness and stability of a protein or protein-ligand complex during molecular simulations.

As it shown in Figure 2A, the Rg value of PR stabilized at 1.80 nm, then decreased after 50 ns before stabilizing again. In contrast, the Rg values for PR-CRC and PR-THC increased. In Figure 2B, the Rg values for RT, RT-THC, and RT-CRC stabilized at 3.55 nm after 30 ns. In Figure 2C, the Rg value for IN stabilized at 1.58 nm, while the Rg values for IN-THC and IN-CRC stabilized at 1.53 nm after 50 ns.

Overall, Figure 2 indicates that all ligand-protein complexes exhibit lower Rg values compared to the proteins alone. The complex is more stable, indicating the inactivity of the virus.

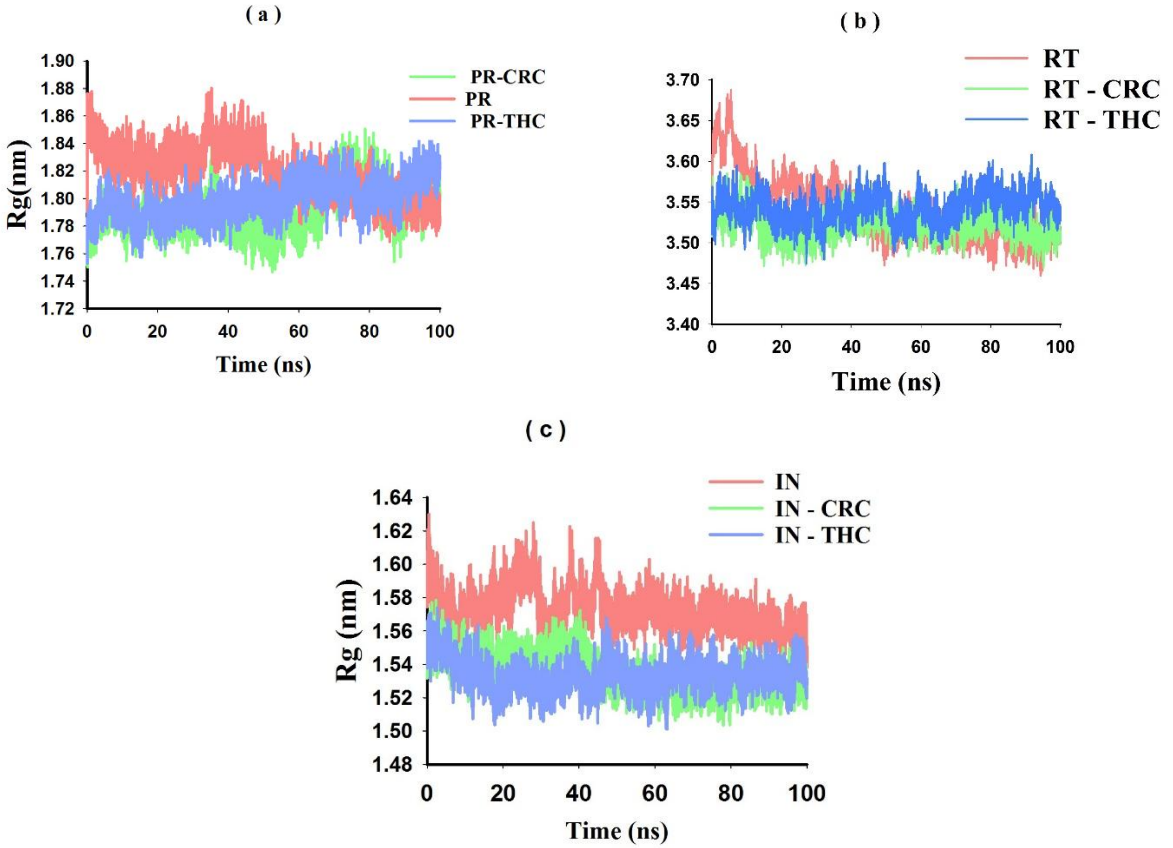

Figure 2: Radius of gyration (Rg). (a) PR, PR-THC and PR-CRC (b) RT, RT-THC and RT-CRC (c) IN, IN-THC and IN-CRC.

Root-mean-square Fluctuation (RMSF)

The flexibility of the HIV-1 protein complexes with two herbal ligands was compared using residue-specific root-mean-square fluctuations (RMSF). Figure 3 shows the flexibility of residues during the simulation.

As shown in Figure 3A, the RMSF values of PR, PR-CRC, and PR-THC were compared. The RMSF of PR-THC is greater than that of both PR and PR-CRC. Additionally, atomic fluctuations at the flap top residues (Ile50/50′) are higher in all complexes. The RMSF values of RT, RT-CRC, and RT-THC are shown in Figure 3B, where the average RMSF value of THC is greater than that of CRC. Residues THR 696 and LYS 103 form hydrogen bonds with CRC, so these regions exhibit less fluctuation compared to THC, which does not form any hydrogen bonds with RT.

Figure 3C presents the RMSF values of IN, IN-THC, and IN-CRC. Both ligands, CRC and THC, form hydrophobic interactions with the LYS101 residue, resulting in similar RMSF graphs for both ligands. Based on the RMSF plots, the complexes with THC show greater RMSF values than those with CRC. Therefore, it can be concluded that the THC ligand induces more inhibition of HIV-1 activity.

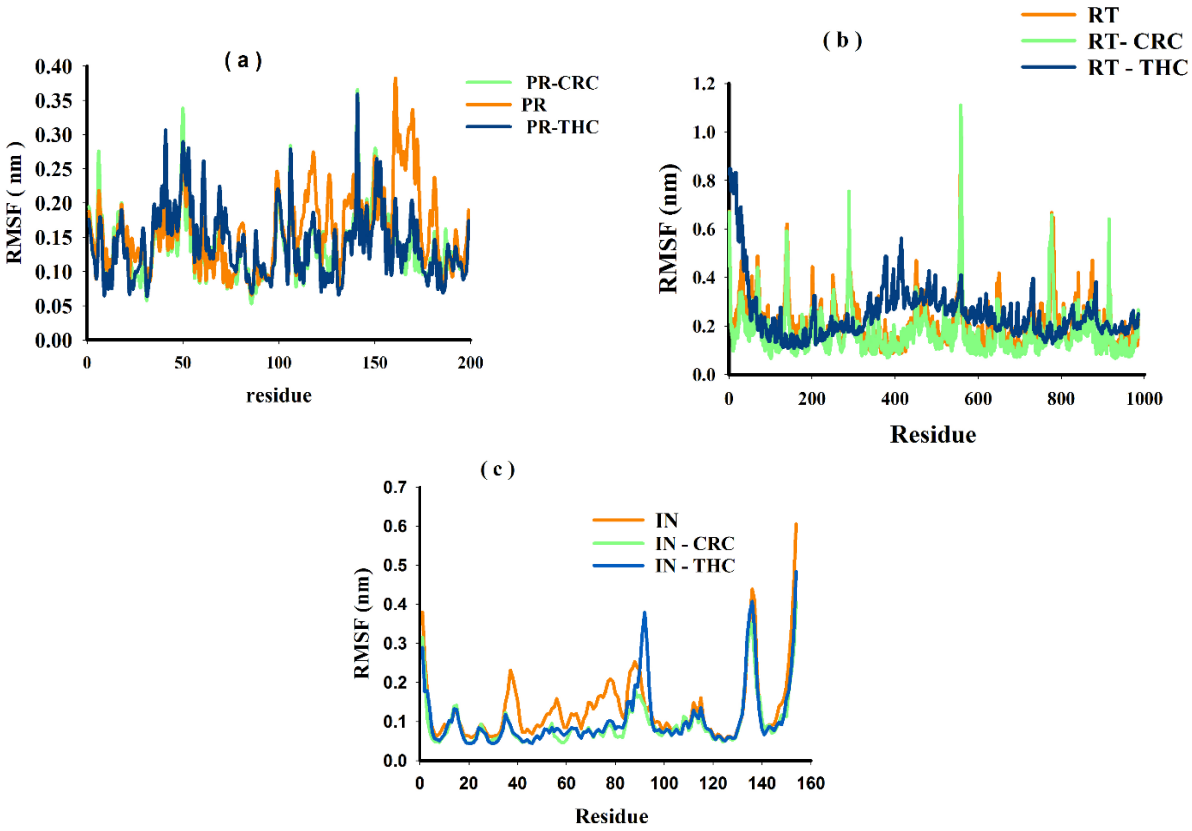

Figure 3: The root-mean-square fluctuation (RMSF) values of (a) PR, PR-CRC and PR-THC (b) RT, RT-CRC and RT-THC (c) IN, IN-CRC and IN-THC.

Solvent Accessible Surface Area (SASA)

The solvent-accessible surface area (SASA) of proteins is an important factor in studies of protein stability and folding. It is defined as the surface surrounding a protein, determined by a hypothetical solvent sphere centered on the van der Waals surface of the molecule. Figure 4A shows that the SASA values for PR, PR-CRC, and PR-THC change during the 100 ns MD simulation, with areas of 125 ± 5 nm², 115 ± 5 nm², and 108 ± 2 nm², respectively. The SASA values for the RT, RT-THC, and RT-CRC complexes are shown in Figure 4B, with values of 580 ± 10 nm², 570 ± 10 nm², and 560 ± 10 nm², respectively. Figure 4C displays the SASA for IN, IN-CRC, and IN-THC, with values of 100 ± 10 nm², 95 ± 10 nm², and 90 ± 10 nm², respectively. The solvent-accessible surface area of the protein complex with THC is smaller than that of the complex with CRC, indicating that THC can cover the active sites of proteins more effectively than the other ligands.

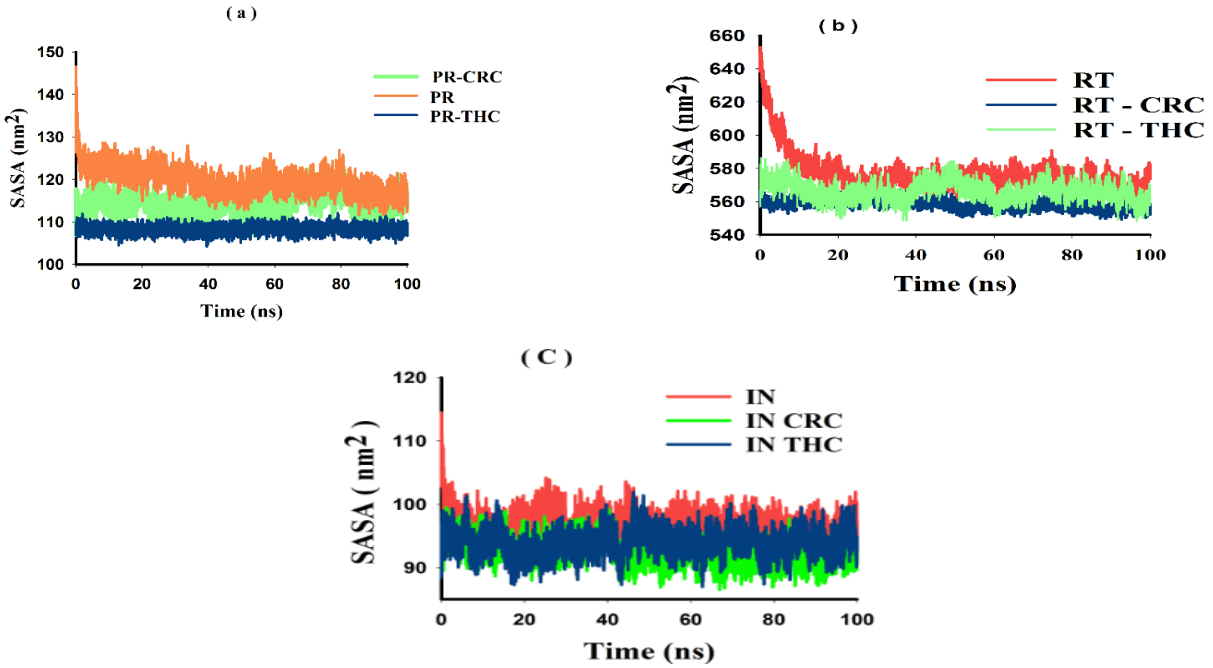

Figure 4: SASA of PR, PR-CRC and PR-THC in the 100 ns simulations (a). SASA of RT, RT-CRC and RT-THC (b). SASA of IN, IN-CRC and IN-THC (c).

Dictionary of Secondary Structure of Proteins (DSSP)

The DSSP analysis revealed fluctuations among coil, β-sheet, β-bridge, bend, turn, α-helix, and 3-helix structures during the MD simulation. The comparative results of the DSSP analysis for PR, RT, and IN with the two ligands are shown in Table 1. PR-CRC and PR-THC exhibited similar amounts of secondary structure. Additionally, the secondary structure values for RT-THC and RT-CRC were comparable. Similarly, IN-CRC and IN-THC displayed similar DSSP structures. As shown in Table 1, the complexes of the two ligands, CRC and THC, maintain the same secondary structures, suggesting that the type of ligand does not affect the secondary structure of the protein.

Table 1: Percentage of the secondary structure of PR, RT-CRC and IN at binding of CRC and THC.

	CRC			THC		
Percentage of secondary structure	**PR**	**RT**	**IN**	**PR**	**RT**	**IN**
Coil	0.19	0.28	0.17	0.19	0.28	0.17
B-Sheet	0.55	0.19	0.17	0.55	0.19	0.17
B-Bridge	0	0.02	0.01	0	0.02	0.01
Bend	0.12	0.11	0.09	0.12	0.11	0.1
Turn	0.09	0.11	0.12	0.09	0.11	0.14
A-Helix	0.05	0.26	0.43	0.05	0.27	0.41
3-Helix	0	0	0	0	0	0.01
5-Helix	-	0.04	-	-	0.04	-
Structure	0.68	0.58	0.74	0.69	0.58	0.73

Principal Component Analysis (PCA)

One of the advanced methods in MD simulations is principal component analysis (PCA). PCA analyzes protein motions as a mixture of collective movements and local fluctuations. The trajectories of the PR, RT, and IN complexes were obtained using GROMACS software. The PCA graph was calculated using the g_covar and g_anaeig commands to assess the overall motion of the proteins (41), with collective movement derived from all paths using Cα atoms (27). The PCA graph is generated by plotting eigenvectors (eigenvectors 1 and 2, or PCA1 vs. PCA2), which exhibit the maximum motion of the protein. The eigenvalue is a key property of the covariance matrix and reflects the energetic contribution of all motions. Eigenvectors are used to evaluate the orientation of atomic movement in the compositional phase. The eigenvector with the largest eigenvalue is referred to as the "principal component."

The covariance trace values for the PR, PR-CRC, and PR-THC complexes are 4.01286 nm^2, 2.489 nm^2, and 2.733 nm^2, respectively. The effect of the CRC and THC ligands on PR binding results in observable changes in the overall motion of PR within conformational space, as shown in Figure 5A. The covariance trace values for the RT, RT-CRC, and RT-THC complexes are 41.066 nm^2, 29.68 nm^2, and 35.34 nm^2, respectively. Figure 5B displays the PCA plots of RT with CRC and THC ligands. The covariance trace values for the IN, IN-CRC, and IN-THC complexes are 3.813 nm^2, 2.0445 nm^2, and 2.7319 nm^2, respectively. Figure 5C presents the PCA plots of IN with CRC and THC ligands. These results illustrate that the THC ligand has greater covariance trace values with proteins compared to CRC, indicating that THC is a better ligand than CRC.

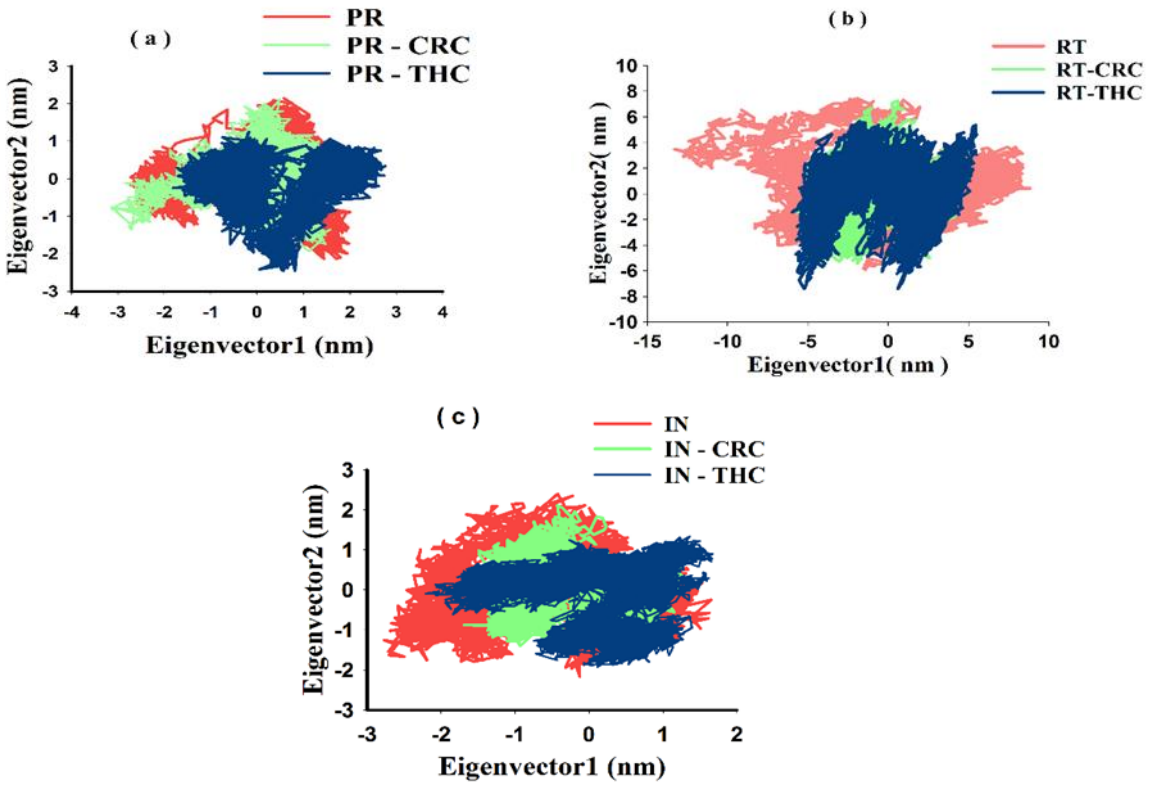

Figure 5: PCA plot created by projection on eigenvector 1 vs projection eigenvector2. (a) PCA plot of PR, PR-CRC and PR-THC (b) PCA plot of RT, RT-CRC and RT-THC (c) PCA plot of IN, IN-CRC and IN-THC.

Binding Free Energy Calculation: g_mmpbsa

The binding free energy was calculated using the g_mmpbsa tool (42). G_mmpbsa is a developed tool that offers improved efficiency for trajectory analysis and the calculation of specific energy. Additionally, g_mmpbsa provides information on the molecular surface during the calculation of solvation energy for both polar and nonpolar solvents (43). Polar solvation energy is calculated using the Poisson-Boltzmann (PB) method (44,45), while nonpolar solvation energy is derived from the solvent-accessible surface area (SASA) model. The dielectric constant for the solvent is set to 80, and for the solute, it is set to 4.

$\Delta G_{binding} = G_{complex} - (G_{receptor} + G_{ligand})$

To evaluate the binding free energy of the PR, RT, and IN complexes using the MM/PBSA method, trajectories from molecular dynamics simulations were analyzed. The binding free energy and its corresponding components obtained from the MM/PBSA calculations for the PR, RT, and IN complexes with the two ligands are summarized in Table 2. The results indicate that the binding free energies of all three proteins with the two ligands are negative. Furthermore, electrostatic interactions, van der Waals forces, SASA, and polar solvation

energy negatively contribute to the total interaction energy, while only polar solvation energy positively contributes to the total binding free energy. The relative binding free energies of the three proteins with the two ligands support strong binding within the dynamic system. According to Table 2, the total binding free energy of the THC ligand is more negative than that of the CRC ligand, indicating that the THC ligand has a stronger inhibitory effect than CRC. Table 2: The binding free energy (kcal/mol) is calculated by g_mmpbsa in GROMACS.

Table 2. The binding free energy (kcal/mol) calculated by g_mmpbsa in GROMACS.

	CRC			**THC**		
The energy of a complex system	PR	RT	IN	PR	RT	IN
van der Waals	-140 ± 1.42	-199.248 ± 0.58	-93.969 ± 3.5	-154.2 ± 0.94	-182.353 ± 1	-66.962± 51
Electrostatic	-18.6 ± 0.78	-14.952 ± 0.36	-36.445 ± 1.9	-17.362 ± 1	-14.509 ± 0.785	-3.334 ± 4.9
Polar solvation	94.64 ± 1.3	265.721 ± 148.5	122.937 ± 4. 5	115.99 ± 1.1	95.847 ± 0.67	37.090 ± 19
SASA energy	94.64 ± 1.3	265.721 ± 148.5	122.937 ± 4. 5	115.99 ± 1.1	95.847 ± 0.67	37.090 ± 19
Total binding free energy	-79.87 ± 1.1	29.829 ± 135.85	-18.403 ± 1.5	-73.87 ± 1.6	-120.616 ± 0.940	-40.951± 54

Discussion

In this study, two herbal ligands, curcumin (CRC) and tetrahydrocannabinol (THC) were investigated for their potential to inhibit the HIV-1 virus. The inhibitory activity of these ligands was evaluated by their interactions with three key HIV-1 proteins: protease (PR), reverse transcriptase (RT), and integrase (IN). Molecular dynamics (MD) simulations were performed for six systems—PR-CRC, PR-THC, RT-CRC, RT-THC, IN-CRC, and IN-THC—over 100 ns. The RMSD plots for PR, RT, and IN, both in the absence and presence of the two drugs, show a similar pattern to non-competitive inhibitors. These inhibitors hinder the structural changes of the enzymes, allowing the drugs to remain bound to the proteins throughout the simulation and preventing the enzymes from undergoing maximal structural alterations. Consequently, the RMSD of the proteins decreases in the presence of the drugs.

The radius of gyration (Rg) plots reveal that the Rg values of the proteins increase in the presence of the drugs compared to the proteins alone, suggesting protein unfolding and a subsequent decrease in enzymatic activity. THC induces a more significant increase in Rg compared to CRC, indicating that THC is more effective at altering the tertiary structure of the proteins and causing greater unfolding than

CRC. The RMSF analysis shows that the fluctuation in protein structure, especially at the active sites, decreases in the presence of the drugs.

Additionally, the solvent-accessible surface area (SASA) results indicate that all three proteins have a lower SASA in the presence of THC, as it can cover the active sites of the proteins more effectively, leading to a greater reduction in protein activity. On the other hand, the G_mmpbsa binding energy comparison reveals that the protein complexes with THC have a more negative binding free energy compared to CRC. This suggests that THC has a stronger binding affinity and is a more effective inhibitor than CRC.

References

1.Srivastava HK, Sastry GN. Molecular dynamics investigation on a series of HIV protease inhibitors: assessing the performance of MM-PBSA and MM-GBSA approaches. J Chem Inf Model. 2012; 52(11) :3088–98. doi: 10.1021/ci300385h

2.Ruiz-Pernía JJ, Alves CN, Moliner V, Silla E, Tuñón I. A QM/MM study of the reaction mechanism for the 3′-processing steps catalyzed by HIV-1 integrase. J Mol Struct THEOCHEM. 2009;898(1–3):115–20.

3.Esposito D, Craigie R. HIV integrase structure and function. In: Advances in virus research. Elsevier; 1999. p.319–33.doi: 10.1016/s0065-3527(08)60304-8

4.Asante-Appiah E, Skalka AM. HIV-1 integrase: structural organization, conformational changes, and catalysis. In: Advances in virus research. Elsevier; 1999. p.351–69.doi: 10.1016/s0065-3527(08)60306-1

5.Chiu TK, Davies DR. Structure and Function of HIV-1 Integrase [Internet]. Bentham Science Publishers; 2004 [cited 2020 Apr 26]. Available from: https://www.ingentaconnect.com/content/ben/ctmc/2004/00000004/00000009/art00007

6.Anthony NJ. HIV-1 integrase: a target for new AIDS chemotherapeutics. Curr Top Med Chem. 2004;4(9):979–90. doi: 10.2174/1568026043388448.

7.Chen Z, Li Y, Chen E, Hall DL, Darke PL, Culberson C, et al. Crystal structure at 1.9-A resolution of human immunodeficiency virus (HIV) II protease complexed with L-735,524, an orally bioavailable inhibitor of the HIV proteases. J Biol Chem. 1994;269(42):26344–8.

8.Kohlstaedt LA, Wang J, Friedman JM, Rice PA, Steitz TA. Crystal structure at 3.5 A resolution of HIV-1 reverse transcriptase complexed with an inhibitor. Science. 1992;256(5065):1783–90. doi: 10.1126/ science.1377403

9.Louis JM, Webert IT, Tözsér J, Clore GM, Gronenborn AM. HIV-I protease: Maturation, enzyme specificity, and drug resistance. In: Advances in pharmacology. Elsevier; 2000. p. 111–46. doi: 10.1016/s1054-3589(00)49025-3

10.Oroszlan S, Luftig RB. Retroviral proteinases. In: Retroviruses. Springer; 1990. p. 153–85.

11.Louis JM, Ishima R, Torchia DA, Weber IT. HIV-1 protease: structure, dynamics, and inhibition. Adv Pharmacol. 2007; 55:261–98. doi: 10.1016/S1054-3589(07)55008-8

12.Chang CE, Shen T, Trylska J, Tozzini V, McCammon JA. Gated binding of ligands to HIV-1 protease: Brownian dynamics simulations in a coarse-grained model. Biophys J. 2006;90(11):3880–5. doi: 10.1529/biophysj.105.074575

13.Karplus M, Kuriyan J. Molecular dynamics and protein function. Proc Natl Acad Sci. 2005;102(19):6679–85. doi: 10.1073/ pnas.0408930102

14.Rick SW, Topol IA, Burt SK, Erickson JW. Molecular mechanisms of resistance: Free energy calculations of mutation effects on inhibitor binding to HIV-1 protease. Protein Sci. 1998;7(8):1750–6. doi: 10.1002/pro.5560070809

15.Lepšík M, Kříž Z, Havlas Z. Efficiency of a second-generation HIV-1 protease inhibitor studied by molecular dynamics and absolute binding free energy calculations. Proteins Struct Funct Bioinforma. 2004;57(2):279–93. doi: 10.1002/prot.20192

16.Zoete V, Michielin O, Karplus M. Protein-

ligand binding free energy estimation using molecular mechanics and continuum electrostatics. Application to HIV-1 protease inhibitors. J Comput Aided Mol Des.2003;17(12):861–80. doi: 10.1023/ b:jcam. 0000021882.99270.4c

17.Wang W, Kollman PA. Computational study of protein specificity: the molecular basis of HIV-1 protease drug resistance. Proc Natl Acad Sci. 2001;98(26):14937–42. doi: 10.1073/pnas.251265598

18.Zhao H, Caflisch A. Molecular dynamics in drug design. Eur J Med Chem. 2015; 91:4–14. doi: 10.1016/j.ejmech.2014.08.004

19.Massova I, Kollman PA. Combined molecular mechanical and continuum solvent approach (MM-PBSA/GBSA) to predict ligand binding. Perspect Drug Discov Des. 2000;18(1):113–35. doi: https://doi.org/10.1023/A:1008763014207

20.Baron R, McCammon JA. Molecular Recognition and Ligand Association. Annu Rev Phys Chem. 2013;64(1):151–75. doi: 10.1146/annurev-physchem-040412-110047

21. S. Esmaeili, H. Mosaddeghi, and F. Ravari. Molecular Docking Studies of HIV-1 Protease-, Integrase- and Reverse-Transcriptase with Delta-9-tetrahydrocannabinol and Curcumin as Two Herbal Ligands. Journal of Evolutionary Biochemistry and Physiology, 2021, Vol. 57, No. 2, :281–288. doi: 10.1134/S0022093021020101.

22.Welcome to the GROMACS documentation! — GROMACS 5.1.4 documentation [Internet]. [cited 2020 May 11]. Available from: http: //manual. gromacs.org/documentation/5.1.4/index.html

23.Showalter SA, Brüschweiler R. Validation of Molecular Dynamics Simulations of Biomolecules Using NMR Spin Relaxation as Benchmarks: Application to the AMBER99SB Force Field. J Chem Theory Comput. 2007 May 1;3(3):961–75. doi: 10.1021/ct7000045

24.Yoneya M, Yamaguchi T, Sato S, Fujita M. Simulation of metal–ligand self-assembly into spherical complex M6L8. J Am Chem Soc. 2012;134(35):14401–7. doi: 10.1021/ja303542r

25.Bayly CI, Cieplak P, Cornell W, Kollman PA. A well-behaved electrostatic potential based method using charge restraints for deriving atomic charges: the RESP model. J Phys Chem. 1993;97(40):10269–80. doi: 10.1021/j100142a004v

26.Mark P, Nilsson L. Structure and Dynamics of the TIP3P, SPC, and SPC/E Water Models at 298 K. J Phys Chem A. 2001 Nov;105(43):9954–60. doi: 10.1021/jp003020w

27.Martoňák R, Laio A, Parrinello M. Predicting Crystal Structures: The Parrinello-Rahman Method Revisited. Phys Rev Lett. 2003 Feb 20;90(7):075503. doi: 10.1103/PhysRevLett.90.075503

28.Lin JH, Perryman AL, Schames JR, McCammon JA. Computational drug design accommodating receptor flexibility: the relaxed complex scheme. J Am Chem Soc. 2002;124(20):5632–3. doi: 10.1021/ja0260162

29.Fadrná E, Hladečková K, Koča J. Long-range Electrostatic Interactions in Molecular Dynamics: An Endothelin-1 Case Study. J Biomol Struct Dyn. 2005 Oct;23(2):151–62.doi: 10.1080/ 07391102. 2005. 10531229

30.Przybylski D, Rost B. Predicting simplified features of protein structure. Bioinformatics-From Genomes to Therapies. 2007 Jan 11:261-95. doi: https://doi.org/10.1002/9783527619368.ch9

31.Kumar CV, Swetha RG, Anbarasu A, Ramaiah S. Computational analysis reveals the association of threonine 118 methionine mutation in PMP22 resulting in CMT-1A. Adv Bioinforma. 2014;2014. doi: 10.1155/2014/502618

32.Cloete R, Kapp E, Joubert J, Christoffels A, Malan SF. Molecular modelling and simulation studies of the Mycobacterium tuberculosis multidrug efflux pump protein Rv1258c. PloS One. 2018;13(11): e0207605. doi: 10.1371/journal.pone.0207605

33.Cantin C. Advanced Introduction to UNIX/linux. 2006.

34.Maschauer S, Michel K, Tripal P, Büther K, Kuwert T, Schober O, et al. Synthesis and in vivo evaluation of an 18F-labeled glycoconjugate of PD156707 for imaging ETA receptor expression in thyroid carcinoma by positron emission tomography. Am J Nucl Med Mol Imaging. 2013;3(5):425. https://pmc.ncbi.nlm.nih.gov/articles/PMC3784806/

35.Yarmanda A. VMD Documentation. doi: 10.13140/ RG.2.2.23583.20643

36.Grayson P, Gullingsrud J, Isralewitz B, Norris D, Stone J. VMD User's Guide. 2002;

37.Goddard TD, Huang CC, Ferrin TE. Software

extensions to UCSF chimera for interactive visualization of large molecular assemblies. Structure. 2005;13(3):473–82. doi: 10.1016/j.str.2005.01.006

38.Goddard TD, Huang CC, Ferrin TE. Visualizing density maps with UCSF Chimera. J Struct Biol. 2007;157(1):281–7. doi: 10.1016/ j.jsb.2006.06.010

39.Samorlu AS, Yelekçi K, Ibrahim Uba A. The design of potent HIV-1 integrase inhibitors by a combined approach of structure-based virtual screening and molecular dynamics simulation. J Biomol Struct Dyn. 2019;37(17):4644–50. doi: 10.1080/07391102.2018.1557559

40.Ali MA. Molecular docking and molecular dynamics simulation of anticancer active ligand '3, 5, 7, 3′, 5′- pentahydroxy -flavanono l-3-O-α-L-rhamnopyranoside'from Bauhinia strychnifolia Craib to the cyclin-dependent protein kinase. J King Saud Univ-Sci. 2020;32(1):891–5. doi: 10.1016/ j.jksus. 2019.05.004

41.Anbarasu K, Jayanthi S. Identification of curcumin derivatives as human LMTK3 inhibitors for breast cancer: a docking, dynamics, and MM/PBSA approach. 3 Biotech. 2018;8(5):228. doi: 10.1007/s13205-018-1239-6. Epub 2018 Apr 27.

42.Kumari R, Kumar R, Consortium OSDD, Lynn A. g_mmpbsa A GROMACS tool for high-throughput MM-PBSA calculations. J Chem Inf Model. 2014;54(7):1951–62. doi: 10.1021/ci500020m

43.Rungsung I, Rajagopalan M, Ramaswamy A. Molecular dynamics study of TMPA mediated dissociation of Nur77-LKB1 complex. Comput Biol Chem. 2018 Oct 1; 76:67–78. doi: 10.1016/ j.compbiolchem.2018.06.002

44.Baker NA, Sept D, Joseph S, Holst MJ, McCammon JA. Electrostatics of nanosystems: application to microtubules and the ribosome. Proc Natl Acad Sci. 2001;98(18):10037–41. doi: 10.1073/pnas.181342398

45.Honig B, Nicholls A. Classical electrostatics in biology and chemistry. Science. 1995; 268(5214):1144–9. doi: 10.1126/ science. 7761829.